Volume 24
Number 24
21 December 2022
Pages 9333-9784

Green Chemistry

Cutting-edge research for a greener sustainable future

rsc.li/greenchem

ISSN 1463-9262

ROYAL SOCIETY OF CHEMISTRY

PAPER

Richard J. Lewis, Graham J. Hutchings *et al.*
Cyclohexanone ammoximation *via in situ* H_2O_2 production using TS-1 supported catalysts

Green Chemistry

PAPER

View Article Online
View Journal | View Issue

Cite this: *Green Chem.*, 2022, **24**, 9496

Cyclohexanone ammoximation *via in situ* H_2O_2 production using TS-1 supported catalysts†

Richard J. Lewis, *[a] Kenji Ueura, [b] Yukimasa Fukuta, [b] Thomas E. Davies,[a] David J. Morgan, [a,c] Charlie B. Paris,[d] James Singleton,[a] Jennifer. K. Edwards, [d] Simon J. Freakley,[e] Yasushi Yamamoto[b] and Graham J. Hutchings *[a]

Received 19th July 2022,
Accepted 8th September 2022

DOI: 10.1039/d2gc02689a

rsc.li/greenchem

The ammoximation of cyclohexanone to the corresponding oxime *via in situ* H_2O_2 formation offers an attractive alternative to the current industrial means of production, overcoming the significant economic and environmental concerns associated with the manufacture of a key reagent, H_2O_2. Herein we demonstrate the efficacy of a composite catalyst, consisting of precious metal nanoparticles supported on a commercial TS-1, towards the *in situ* synthesis of cyclohexanone oxime, bridging the wide condition gap that exists between the two distinct reaction pathways: H_2O_2 direct synthesis and cyclohexanone ammoximation. In particular, the alloying of Au with Pd and the introduction of low concentrations of Pt into AuPd nanoalloys are found to be key in promoting high catalytic performance. The improved catalytic activity of optimal catalysts is found to result from a combination of a disruption of contiguous Pd ensembles and the modification of Pd oxidation states, which in turn dictate catalytic activity towards the production and subsequent degradation of H_2O_2.

Introduction

The ammoximation of cyclohexanone to cyclohexanone oxime is a key process in the production of Nylon-6, with annual global production of the polyamide predicted to reach 8.9 million tons by 2024, a concurrent increase in the demand for cyclohexanone oxime is likewise expected.[1] The application of the titanosilicate TS-1, first developed by EniChem,[2] in conjunction with preformed H_2O_2 and NH_3 overcame many of the drawbacks associated with the traditional route to oxime production, chiefly the formation of large quantities of the low-value fertilizer, ammonium sulphate. Key to the efficacy of the EniChem route is the high co-ordination ability of Ti^{IV} sites present within the TS-1 framework, which are considered responsible for the formation of the hydroxylamine intermediate from H_2O_2 and NH_3, which subsequently reacts with cyclohexanone to produce the oxime with high selectivity.[3]

Although the H_2O_2/TS-1 approach is able to achieve high selectivity towards cyclohexanone oxime, there are still significant improvements that can be achieved through decoupling the ammoximation process from the industrial means of H_2O_2 production, the anthraquinone oxidation process. Indeed, like all processes that utilise preformed H_2O_2 there are considerable economic and environmental costs associated with transport and storage, with the energy utilised in concentration of the oxidant effectively wasted upon dilution of the oxidant to appropriate levels prior to use.[4] Additionally, the instability of H_2O_2 even at relatively mild temperatures requires the use of acidic stabilizing agents to prevent decomposition to H_2O,[5] with such promoters able to promote both decreased reactor and catalyst longevity as well as leading to the formation of complex product streams, adding significant cost to any industrial process.[6]

The direct synthesis of H_2O_2 from molecular H_2 and O_2 has been well reported in the literature, with AuPd-based catalysts in particular well studied,[7–9] indeed there is growing interest in the use of such materials to generate H_2O_2 *in situ* for the selective oxidation of a range of chemical feedstocks.[10–16] However, such approaches have yet been unable to demonstrate a viable alternative to the existing industrial processes they aim to replace, often suffering from relatively low rates of conversion and selectivity based on H_2.[17] Additionally, the generation of considerable quantities of undesirable by-products, often driven by the presence of the H_2 required to produce H_2O_2 is a cause for concern, with the utilisation of

[a]*Max Planck–Cardiff Centre on the Fundamentals of Heterogeneous Catalysis FUNCAT, Cardiff Catalysis Institute, School of Chemistry, Cardiff University, Main Building, Park Place, Cardiff, CF10 3AT, UK. E-mail: LewisR27@cardiff.ac.uk, Hutch@cardiff.ac.uk*
[b]*UBE Corporation, 1978-5, Kogushi, Ube, Yamaguchi 755-8633, Japan*
[c]*HarwellXPS, Research Complex at Harwell (RCaH) Didcot, OX11 0FA, UK*
[d]*Cardiff Catalysis Institute, School of Chemistry, Cardiff University, Main Building, Park Place, Cardiff, CF10 3AT, UK*
[e]*Department of Chemistry, University of Bath, Claverton Down, Bath, BA2 7AY, UK*
†Electronic supplementary information (ESI) available. See DOI: https://doi.org/10.1039/d2gc02689a

inhibitors to suppress competitive side reactions, which add further complexity to the process, typical.[15,17]

Recently we reported that through the *in situ* production of H_2O_2 from molecular H_2 and O_2 it is possible to catalyse the ammoximation of a range of ketones to the corresponding oxime, with product selectivities comparable to the current industrial route of production, while also achieving high utilisation of H_2.[18] This earlier investigation, focussed on a wet impregnation approach to catalyst synthesis, due in part to its simplicity and industrial applicability. However, such routes to catalyst preparation often fail to achieve high dispersion of active metals and in the case of bi-metallic systems can lead to incomplete alloy formation and inhomogeneity between nanoparticles.[19,20] Furthermore, a significant focus of this earlier work was placed on the use of a physical mixture of TS-1 in conjunction with AuPd nanoparticles supported on a secondary carrier, however for industrial application a single-phase composite catalyst would clearly be preferential.

The solution phase formation of nanoalloys prior to their immobilisation onto a carrier has been widely demonstrated to offer enhanced control of particle size, shape and composition[21–23] when compared to alternative routes to catalyst synthesis such as wet impregnation. Typically colloidal approaches involve the rapid chemical reduction of metal precursor species and the inhibition of particle agglomeration through the use of capping agents, with the application of such species, often reported to result in the modification of catalyst reactivity through steric effects and modification of metal oxidation states.[23–25]

With this in mind and in an attempt to better utilise precious metal sites and further improve on the rate of cyclohexanone ammoximation we have recently reported, within this current study we have evaluated the efficacy of TS-1 immobilised AuPd nanoparticles, synthesised by a facile sol-immobilisation technique,[26] towards the *in situ* ammoximation of cyclohexanone to the corresponding oxime.

Experimental

Catalyst preparation

Mono-, bi- and tri-metallic 0.66%AuPdPt/TiO_2 catalysts have been prepared (on a weight basis) by a sol-immobilisation procedure, based on a methodology previously reported in the literature,[22] which has been shown to result in enhanced precious metal dispersion by limiting particle growth, while also allowing for improved interaction between active metal components.[23,26] The procedure to produce the 0.275%Au–0.275%Pd–0.11%Pt/TS-1 catalyst (2 g) is outlined below with a similar methodology utilised for all catalysts.

Aqueous solutions of $HAuCl_4{\cdot}3H_2O$ (0.449 mL, [Au] = 12.25 mg mL^{-1}, Strem Chemicals), $PdCl_2$ (0.917 mL, [Pd] = 6.0 mg mL^{-1}, Merck) and $H_2PtCl_6{\cdot}3H_2O$ (0.231 mL, [Pt] = 9.5 mg mL^{-1}, Merck), were added to deionised water (800 mL) under vigorous stirring, at room temperature. The resulting solution was allowed to stir for 2 minutes prior to the addition of polyvinylalcohol (PVA) (1.584 mL, 1 wt.% MW = 9000–10 000 g mol^{-1}, 80% hydrolysed, Merck) such that the weight ratio of metal : PVA was 1 : 1.2, unless otherwise stated. The resulting solution was stirred for 2 minutes prior to the addition of a freshly prepared solution of $NaBH_4$ (4.776 mL, 0.1 M, Merck), such that the molar ratio of $NaBH_4$: (Au + Pd) was 5 : 1 and the molar ratio of $NaBH_4$: Pt was 10 : 1. Upon the addition of $NaBH_4$ the mixture turned dark brown and was stirred vigorously for an additional 30 minutes followed by the addition of TS-1 (1.987 g, HighChem). The solution was acidified to pH 1 *via* the addition of H_2SO_4 (>95%, Fischer Scientific) and allowed to stir for a further 1 h. The need for acidification of the catalyst synthesis solution can be related to the kinetics of nanoalloy immobilisation, through acidification it is possible to promote deposition of the PVA-encapsulated metal species and therefore good control over nanoparticle size. Following this, the suspension was filtered under vacuum, washed thoroughly with distilled water until the pH of the washings were neutral, then dried (110 °C, 16 h, static air). The resulting material was subsequently ground and calcined (400 °C, 3 h, 10 °C min^{-1}, static air), unless otherwise stated.

The TS-1 utilised in this study was provided by HighChem and manufactured by Hengyi Chemical (Batch number 17052, manufacturer website: **https://www.hengyichemical.com/product/36-en.html**).

Catalyst testing

Note 1: Reaction conditions used within this study operate below the flammability limits of gaseous mixtures of H_2 and O_2.

Note 2: The conditions used within this work for H_2O_2 synthesis and degradation have previously been investigated, with the presence of CO_2 as a diluent for reactant gases and a methanol co-solvent identified as key to maintaining high catalytic efficacy towards H_2O_2 production.[27]

Note 3: In all cases reactions were run multiple times, over multiple batches of catalyst, with the data presented being an average of these experiments.

Direct synthesis of H_2O_2

Hydrogen peroxide synthesis was evaluated using a Parr Instruments stainless steel autoclave with a nominal volume of 100 mL, equipped with a PTFE liner and a maximum working pressure of 2000 psi. To test each catalyst for H_2O_2 synthesis, the autoclave was charged with catalyst (0.01 g), solvent (5.6 g MeOH and 2.9 g H_2O, both HPLC grade, Fischer Scientific). The charged autoclave was then purged three times with 5% H_2/CO_2 (100 psi) before filling with 5% H_2/CO_2 (420 psi), followed by the addition of 25%O_2/CO_2 (160 psi) to give a $H_2 : O_2$ ratio of 1 : 2. The temperature was then decreased to 2 °C (using a HAAKE K50 bath/circulator and an appropriate coolant) followed by stirring (1200 rpm) of the reaction mixture for 0.5 h. Gas pressures are given as gauge pressures, the reagents were not continuously introduced into the reactor. The above reaction parameters represent the optimum conditions we have previously used for the synthesis of

H_2O_2.[24] H_2O_2 productivity was determined by titrating aliquots of the final solution after reaction with acidified $Ce(SO_4)_2$ (0.01 M) in the presence of ferroin indicator. Catalyst productivities are reported as $mol_{H2O2}\ kg_{cat}^{-1}\ h^{-1}$.

Degradation of H_2O_2

Catalytic activity towards H_2O_2 degradation (*via* hydrogenation and decomposition pathways) was determined in a manner similar to that used for measuring the H_2O_2 direct synthesis activity of a catalyst. The autoclave was charged with methanol (5.6 g, HPLC grade, Fisher Scientific), H_2O_2 (50 wt% 0.69 g, Merck), H_2O (2.21 g, HPLC grade, Fisher Scientific) and catalyst (0.01 g), with the solvent composition equivalent to a 4 wt. % H_2O_2 solution. From the solution, two aliquots of 0.05 g were removed and titrated with acidified $Ce(SO_4)_2$ solution using ferroin as an indicator to determine an accurate concentration of H_2O_2 at the start of the reaction. The charged autoclave was then purged three times with 5%H_2/CO_2 (100 psi) before filling with 5%H_2/CO_2 (420 psi). Gas pressures are given as gauge pressures, the reagents were not continuously introduced into the reactor. The reaction mixture was cooled to 2 °C prior to the reaction commencing upon stirring (1200 rpm). The reaction was allowed to proceed for 0.5 h, after which, the catalyst was removed from the reaction solvents *via* filtration and as described previously, two aliquots of 0.05 g were titrated against the acidified $Ce(SO_4)_2$ solution using ferroin as an indicator. Catalyst degradation activity is reported as $mol_{H2O2}\ kg_{cat}^{-1}\ h^{-1}$.

Cyclohexanone ammoximation *via* the *in situ* synthesis of H_2O_2

Catalysts were evaluated for their activity towards ketone ammoximation with the procedure for cyclohexanone ammoximation outlined below using a stainless-steel autoclave (Parr Instruments) with a nominal volume of 100 mL, equipped with a PTFE liner and a maximum working pressure of 2000 psi.

The autoclave was charged with the catalyst (0.075 g), solvent (H_2O (7.5 g, HPLC grade, Fisher Scientific) and *t*-BuOH (5.9 g, Merck), cyclohexanone (0.196 g, 2.0 mmol, Merck) and ammonium bicarbonate (0.32 g, 4.0 mmol, Merck). With *t*-BuOH chosen as co-solvent due to enhanced solubility of H_2, in comparison to H_2O, and the ability of *t*-BuOH to aid in the maintenance of the –Ti(IV)–O–Si– moiety, considered to be responsible for the high activity of TS-1.[25] The reactor was purged three times with 5% H_2/N_2 (100 psi) and then filled with 5% H_2/N_2 (420 psi) and 25% O_2/N_2 (160 psi) to give a $H_2:O_2$ ratio of 1 : 2. Reactant gas pressures are reported as gauge pressures, the reagent gases were not continuously introduced into the reactor. The reactor was stirred (100 rpm) while the reaction temperature was raised to 80 °C at which time stirring was increased to 800 rpm. The reaction was allowed to run for 3 h, unless otherwise stated, after which the reactor was cooled to 25 °C while stirring (100 rpm), using ice water. To the reaction solution ethanol (6 g, Fischer Scientific) and diethylene glycol monoethyl ether (0.15 g, Merck) were added, with the former used to ensure the complete homogeneity of the post-reaction solution, while the latter was chosen as an external standard. Following this the catalyst was removed by filtration and the resulting solution was analysed by gas chromatography using a Varian 3800 equipped with FID and a CP-Wax 52 CB column.

Ketone conversion and selectivity towards the oxime were calculated on the basis of starting amount of the ketone, according to eqn (1) and (2), respectively.

$$X_{\text{ketone}} = \frac{n_{\text{ketone}(t(0))} - n_{\text{ketone}(t(1))}}{n_{\text{ketone}(t(0))}} \times 100 \quad (1)$$

$$S_{\text{oxime}} = \frac{n_{\text{oxime}}}{n_{\text{ketone}(t(0))} - n_{\text{ketone}(t(1))}} \times 100. \quad (2)$$

Catalyst characterisation

Investigation of the bulk structure of the crystalline materials was carried out using a (θ–θ) PANalytical X'pert Pro powder diffractometer using a Cu K_α radiation source, operating at 40 KeV and 40 mA. Standard analysis was carried out using a 40 min run with a back filled sample, between 2θ values of 10–80°. Phase identification was carried out using the International Centre for Diffraction Data (ICDD).

X-ray diffractograms of the as-prepared 0.66%AuPd/TS-1 catalysts in Fig. S.1,† with no reflections associated with either Au or Pd observed, indicative of the low total loading and the high dispersion of the immobilised metals, which is typical of the route to catalyst synthesis.

N_2 isotherms were collected on a Micromeritics 3Flex. Samples (*ca.* 0.020 g) were degassed (150 °C, 6 h) prior to analysis. Analyses were carried out at 77 K with P_0 measured continuously. Free space was measured post-analysis with He. Pore size analysis was carried out using Micromeritics 3Flex software, N_2-Cylindrical Pores-Oxide Surface DFT Model.

Note 4: Surface area analysis of the as received TS-1 and 0.33%Au–0.33%Pd/TS-1 (PVA : metal = 1.2) catalyst exposed to an oxidative heat treatment (static air, 400 °C, 3 h) is reported in Fig. S.2,† with a minor reduction in both surface area and pore volume observed with the immobilisation of precious metals onto the TS-1 support and subsequent exposure to an oxidative heat treatment.

X-ray photoelectron spectroscopy (XPS) analyses were made on a Kratos Axis Ultra DLD spectrometer. Samples were mounted using double-sided adhesive tape and binding energies were referenced to the C (1s) binding energy of adventitious carbon contamination that was taken to be 284.8 eV. Monochromatic AlK_α radiation was used for all measurements; an analyser pass energy of 160 eV was used for survey scans while 40 eV was employed for detailed regional scans. The intensities of the Au(4f) and Pd(3d) features were used to derive the Au/Pd surface composition ratios. All transmission function corrected data was processed using CasaXPS v2.3.2 after removal of a Shirley background using modified Wagner sensitivity factors as supplied by the instrument manufacturer.

Fitting of the spectra was performed using Voigt functions the parameters, which were derived from bulk materials.

Transmission electron microscopy (TEM) and scanning transmission electron microscopy (STEM) were performed on a JEOL JEM-2100 operating at 200 kV. Samples were prepared by dispersion in ethanol *via* sonication and deposited on 300 mesh copper grids coated with holey carbon film.

Thermal gravimetric analysis (TGA) was performed using a PerkinElmer TGA 4000. Catalytic samples (*ca.* 20–30 mg) were loaded into a ceramic crucible and then heated to 800 °C (5 °C min^{-1}) under a flow of air (50 mL min^{-1}).

Metal leaching was quantified using an Agilent 7900 ICP-MS equipped with an I-AS auto-sampler using a 5-point calibration using certified reference materials from PerkinElmer and certified internal standard from Agilent. All calibrants were matrix matched.

Results and discussion

Our initial studies established the efficacy of TS-1 supported precious metal catalysts towards the direct synthesis of H_2O_2 and its subsequent degradation, *via* hydrogenation and decomposition pathways, under conditions previously optimised for H_2O_2 synthesis. These include the presence of sub-ambient reaction temperatures, a methanol co-solvent and CO_2 gaseous diluent, all of which have been shown to inhibit H_2O_2 degradation pathways and promote H_2O_2 stability (Table S.1†).[27] In keeping with previous investigations,[9,28–30] the incorporation of Au into supported Pd nanoparticles, so that Au and Pd content were equal on a weight basis, was observed to lead to a significant enhancement in catalytic activity towards H_2O_2 synthesis (104 mol_{H2O2} kg_{cat}^{-1} h^{-1}) compared to the analogous monometallic Au- (9 mol_{H2O2} kg_{cat}^{-1} h^{-1}) and Pd-only (12 mol_{H2O2} kg_{cat}^{-1} h^{-1}) catalysts. The synergistic enhancement that results from the alloying Au and Pd has been well reported,[31–33] with numerous studies identifying the ability of Au to promote the desorption of H_2O_2 as well as reaction intermediates (*OH and *OOH) from catalytic surfaces.[33,34] Notably the activity of the 0.33%Au–0.33%Pd/TS-1 catalyst investigated within this study significantly exceeds that recently reported for the analogous catalyst formulation prepared *via* a wet co-impregnation procedure (44 mol_{H2O2} kg_{cat}^{-1} h^{-1}) highlighting a key benefit of the sol-immobilisation route to catalyst synthesis.[18]

Subsequent evaluation of catalytic performance towards cyclohexanone ammoximation, under conditions considered to be detrimental towards H_2O_2 production, namely the presence of ammonia and elevated temperatures,[35] revealed the limited activity of both the monometallic Au and Pd catalysts towards cyclohexanone oxime production (3 and 13% oxime yield respectively). In comparison, the 0.33%Au–0.33%Pd/TS-1 catalyst (66% oxime yield) was observed to be far superior to the monometallic analogues (Fig. 1), which, alongside our studies into the direct synthesis of H_2O_2 (Table S.1†) highlights the key role of AuPd nanoalloy formation.

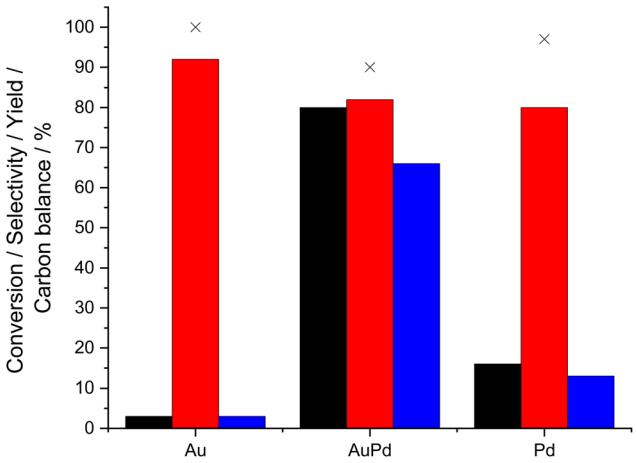

Fig. 1 Catalytic activity of 0.66%AuPd/TS-1 catalysts prepared *via* sol-immobilisation towards the ammoximation of cyclohexanone *via in situ* production of H_2O_2. Ammoximation reaction conditions: cyclohexanone (2 mmol), NH_4HCO_3 (4 mmol), 5%H_2/N_2 (420 psi), 25%O_2/N_2 (160 psi), catalyst (0.075 g), *t*-BuOH (5.9 g), H_2O (7.5 g), 3 h, 80 °C 800 rpm. Key: cyclohexanone conversion (black bar), selectivity towards oxime (red bar), cyclohexanone oxime yield (blue bar), carbon balance (crosses). Note: all catalysts were exposed to an oxidative heat treatment prior to use (static air, 400 °C, 3 h).

The disruption of contiguous Pd ensembles through the alloying with Au has been widely considered a major underlying cause for the synergy that often results from the combination of these two metals, although other factors, such as the control of Pd oxidation state and nanoparticle morphology clearly also play a role in altering catalytic performance.[36–39] Pertinent to H_2O_2 production, Goodman and co-workers have reported the increased selectivity toward O–O bond maintenance (necessary for the formation of H_2O_2), which can be achieved through the formation of AuPd alloys, with the combination of electronic perturbation and isolation of Pd sites considered to make Pd more "atom-like", and subsequently results in the weaker binding of reactants and products.[40,41] In order to achieve optimal catalytic performance, there is a clear need to balance the dissociation of H_2, favoured over Pd ensembles, with the stability of $*O_2$ and *OOH intermediate surface species, favoured over AuPd alloy surfaces.[42]

We subsequently investigated the effect of the Au : Pd ratio on catalytic activity towards both the direct synthesis of H_2O_2 (Fig. S.3†) and cyclohexanone ammoximation (Fig. 2, with determination of apparent reaction rates reported in Table S.2†). These studies revealed the enhanced activity of the Au-rich 0.44%Au–0.22%Pd/TS-1 catalyst, which offered a H_2O_2 synthesis activity of 115 mol_{H2O2} kg_{cat}^{-1} h^{-1} and cyclohexanone oxime yield of 76%, with both metrics decreasing with the further introduction of Pd. Such a correlation perhaps unsurprisingly may be considered indicative of the direct relationship between the two separate processes (H_2O_2 synthesis and cyclohexanone ammoximation).

Determination of mean particle size *via* transmission electron microscopy (TEM) revealed that differences in catalytic

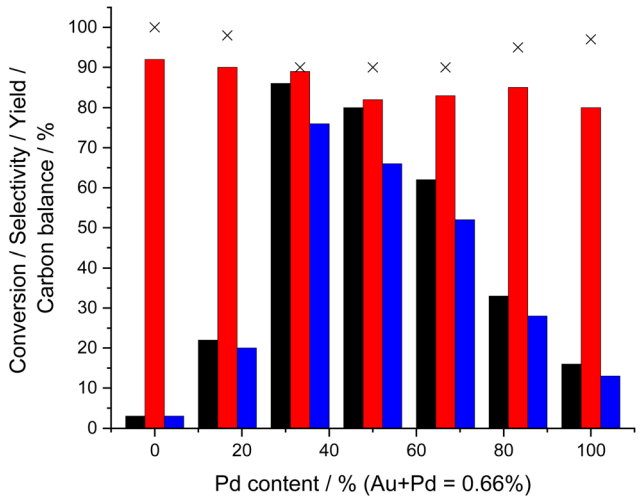

Fig. 2 The effect of Au : Pd ratio on catalytic activity towards the ammoximation of cyclohexanone *via in situ* H_2O_2 production. Ammoximation reaction conditions: cyclohexanone (2 mmol), NH_4HCO_3 (4 mmol), 5%H_2/N_2 (420 psi), 25%O_2/N_2 (160 psi), catalyst (0.075 g), *t*-BuOH (5.9 g), H_2O (7.5 g), 3 h, 80 °C 800 rpm. Key: cyclohexanone conversion (black bar), selectivity towards oxime (red bar), cyclohexanone oxime yield (blue bar), carbon balance (crosses). Note: all catalysts were exposed to an oxidative heat treatment prior to use (static air, 400 °C, 3 h).

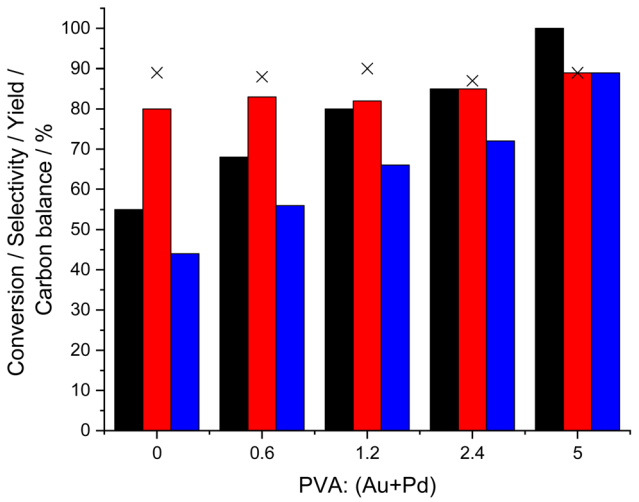

Fig. 3 Effect of PVA : metal ratio on catalytic activity of the 0.33%Au–0.33%Pd/TS-1 catalyst activity towards the ammoximation of cyclohexanone oxime *via in situ* H_2O_2 synthesis. Ammoximation reaction conditions: cyclohexanone (2 mmol), NH_4HCO_3 (4 mmol), 5%H_2/N_2 (420 psi), 25%O_2/N_2 (160 psi), catalyst (0.075 g), *t*-BuOH (5.9 g), H_2O (7.5 g), 3 h, 80 °C 800 rpm. Key: cyclohexanone conversion (black bar), selectivity towards oxime (red bar), cyclohexanone oxime yield (blue bar), carbon balance (crosses). Note: all catalysts were exposed to an oxidative heat treatment prior to use (static air, 400 °C, 3 h).

performance cannot be attributed to variation in this metric, which is an often-key factor in determining catalytic selectivity towards H_2O_2.[43–45] Indeed, good control of particle distribution was observed regardless of nominal catalyst formulation (mean particle size reported in Table 1, with corresponding micrographs reported in Fig. S.4.A and B†), which may have been expected given the chosen route to catalyst synthesis.[23] Analysis of the as-prepared materials *via* X-ray photoelectron spectroscopy (XPS) (Table S.3†), revealed the presence of Pd^0 in all catalysts, despite exposure to an oxidative heat treatment (static air, 400 °C, 3 h). Notably, the Au-rich materials (0.55%Au–0.11%Pd/TS-1 and 0.44%Au–0.22%Pd/TS-1), were found to consist entirely of Pd^0, highlighting the ability of Au to influence Pd speciation. With the known ability of Pd^0 to be highly active toward H_2O_2 synthesis we can attribute the modification of Pd oxidation state to be a key cause of the catalytic performance towards both H_2O_2 production and cyclohexanone ammoximation.

The role of the capping agent on the performance of the 0.33%Au–0.33%Pd/TS-1 catalyst towards both the direct synthesis of H_2O_2 and *in situ* ammoximation of cyclohexanone was next investigated (Table S.4† and Fig. 3 respectively), with numerous studies demonstrating the ability of such ligands to influence catalytic efficiency through control of the three-dimensional environment of the metal active site.[46,47] With catalytic activity towards H_2O_2 synthesis widely reported to be dependent on particle size[43,44,48] it is perhaps understandable that a decrease in this metric upon PVA incorporation during catalyst preparation (Table 2, with corresponding micrographs reported in Fig. S.5†), correlates with a considerable improve-

Table 1 Effect of Au : Pd ratio on the mean particle size of 0.66%AuPd/TS-1 catalysts, prepared *via* sol-immobilisation (PVA : metal = 1.2)

Catalyst	Mean particle size/nm (S.D)	Productivity[a]/mol_{H2O2} kg_{cat}^{-1} h^{-1}	Oxime yield[b]/%
0.66%Au/TS-1	3.4 (0.93)	9	3
0.55%Au–0.11%Pd/TS-1	3.5 (0.79)	20	20
0.44%Au–0.22%Pd/TS-1	3.4 (0.82)	115	76
0.33%Au–0.33%Pd/TS-1	3.4 (1.10)	104	66
0.22%Au–0.44%Pd/TS-1	3.4 (0.80)	86	52
0.11%Au–0.55%Pd/TS-1	2.7 (0.70)	63	28
0.66%Pd/TS-1	3.5 (1.08)	12	13

[a] H_2O_2 direct synthesis reaction conditions: catalyst (0.01 g), H_2O (2.9 g), MeOH (5.6 g), 5% H_2/CO_2 (420 psi), 25% O_2/CO_2 (160 psi), 0.5 h, 2 °C 1200 rpm. [b] Ammoximation reaction conditions: cyclohexanone (2 mmol), NH_4HCO_3 (4 mmol), 5%H_2/N_2 (420 psi), 25%O_2/N_2 (160 psi), catalyst (0.075 g), *t*-BuOH (5.9 g), H_2O (7.5 g), 3 h, 80 °C 800 rpm. Note: all catalysts were exposed to an oxidative heat treatment prior to use (static air, 400 °C, 3 h).

Table 2 Effect of PVA : metal ratio on the mean particle size of 0.33% Au–0.33%Pd/TS-1 catalysts, prepared *via* sol-immobilisation

PVA : metal	Mean particle size/nm (S.D)	Productivity[a]/mol_{H2O2} kg_{cat}^{-1} h^{-1}	Oxime yield[b]/%
0	6.7 (2.51)	56	44
0.6	2.9 (0.74)	82	56
1.2	3.4 (1.10)	104	66
2.4	2.5 (0.77)	136	72
5.0	2.6 (0.72)	165	89

[a] H_2O_2 direct synthesis reaction conditions: catalyst (0.01 g), H_2O (2.9 g), MeOH (5.6 g), 5%H_2/CO_2 (420 psi), 25%O_2/CO_2 (160 psi), 0.5 h, 2 °C, 1200 rpm. [b] Ammoximation reaction conditions: cyclohexanone (2 mmol), NH_4HCO_3 (4 mmol), 5%H_2/N_2 (420 psi), 25%O_2/N_2 (160 psi), catalyst (0.075 g), *t*-BuOH (5.9 g), H_2O (7.5 g), 3 h, 80 °C, 800 rpm. Note: all catalysts were exposed to an oxidative heat treatment prior to use (static air, 400 °C, 3 h).

ment in catalytic performance towards oxime production, with mean nanoparticle size decreasing from 6.7 nm for the catalyst prepared in the absence of PVA (44% oxime yield), to 2.9 nm after PVA introduction (PVA : metal = 0.6) (56% oxime yield). Interestingly, the further addition of PVA during colloid formation was found to result in a significant increase in catalytic activity towards both the direct synthesis of H_2O_2 and the *in situ* ammoximation of cyclohexanone, with the enhanced rate of cyclohexanone conversion particularly notable (100% cyclohexanone conversion and 89% oxime yield observed over the 0.66% AuPd/TS-1 (PVA : metal = 5) catalyst). However, this improvement in catalyst performance does not coincide with a further reduction in mean particle size, which may have been considered the cause for such promotion, with this metric remaining fairly stable (2.5–3.4 nm) for all catalysts prepared in the presence of PVA. In keeping with TEM analysis of this sub-set of materials, further investigation by XPS revealed a broadening of the Au 4f signal with the introduction of PVA, which is indicative of the formation of smaller nanoparticles.[49,50] Additionally, and perhaps more importantly a greater proportion of Pd^0 was also observed with the introduction of increasing amounts of PVA (Fig. S.6†). As such it is possible to attribute the enhanced H_2O_2 synthesis and ammoximation activity of the AuPd/TS-1 catalysts prepared in the presence of the PVA capping agent to result from both a reduction in mean nanoparticle size and, in a manner to our earlier studies into Au : Pd ratio, a shift in Pd oxidation state towards Pd^0.

The utilisation of organic capping agents to both direct nanoparticle morphology and prevent agglomeration is common for colloidal routes to catalyst synthesis. However, in some cases, the resulting organic layer which encapsulates the nanoalloy may inhibit catalyst performance by limiting active site accessibility.[51,52] Notably, this has not been observed for the direct synthesis of H_2O_2, where sol-immobilisation prepared catalysts have been widely studied.[22,47] For those reactions where the presence of the ligand can have deleterious effects, there are many elegant approaches utilised to ensure their removal.[52] Thermal treatment is perhaps the most obvious and can be highly effective even at relatively low temperatures,[53] although both the resulting carbonaceous residues[54] and nanoparticle agglomeration can drastically reduce the performance of the resulting material, particularly in the case of monometallic Pd catalysts.[55] Regardless, the application of thermal treatment is often necessitated to promote catalytic stability through the promotion of strong metal–support interactions (SMSI), which inhibits the leaching of active metals in liquid phase application.[56] Notably in the case of oxide supports SMSI have been attributed to the development of an oxide overlayer, which partially covers metal nanoparticles.[57]

Subsequently, with a focus on the 0.33%Au–0.33%Pd/TS-1 (PVA : metal = 1.2) catalyst, the role of calcination temperature on catalytic performance was next investigated. In keeping with previous studies into AuPd nanoparticles immobilised on a range of supports[58–60] the dried-only material (110 °C, 16 h, static air), offered particularly high activity towards both the direct synthesis (212 mol_{H2O2} kg_{cat}^{-1} h^{-1}) and subsequent degradation (637 mol_{H2O2} kg_{cat}^{-1} h^{-1}) of H_2O_2 (Table S.5†). A minimum calcination temperature of 400 °C was identified to impart catalyst stability, under H_2O_2 direct synthesis conditions (Table S.5†), with earlier studies also revealing the poor stability of AuPd/TS-1 materials calcined at lower temperatures.[60] Perhaps as expected the application of increasing calcination temperatures was also observed to coincide with a reduction in H_2O_2 direct synthesis activity.

Subsequent analysis of the post-reaction solution revealed significant leaching of Pd after use in the H_2O_2 direct synthesis reaction, particularly in the case of the dried-only sample, with this metric decreasing substantially upon exposure to high-temperature calcination (>400 °C) (Table S.6†). By comparison, the extent of Au leaching observed was considerably less and decreased to zero upon exposure to relatively low heat treatment temperatures (>200 °C). Similar observations have been reported for AuPd-supported catalysts for a range of reactions, including H_2O_2 direct synthesis, with the improved stability which results from high-temperature calcination attributed to enhanced metal–support interactions,[56,58] and aligns well with our observations within this study.

Evaluation of catalytic performance towards the *in situ* ammoximation of cyclohexanone (Fig. 4), revealed that despite offering high H_2O_2 synthesis rates the activity of the dried-only material toward the ammoximation reaction was limited (46% cyclohexanone conversion), while exposure to elevated calcination temperatures improved this metric considerably.

In an attempt to identify the underlying relationship between catalyst performance and calcination temperature the dried-only material was subsequently analysed by thermal gravimetric analysis (TGA) (Fig. S.7†), which revealed two distinct regions of interest (0–200 and 200–800 °C). The initial mass loss observed below 200 °C can be associated with the removal of physisorbed water,[61] while that observed at temperatures exceeding 200 °C can be attributed to the thermal decomposition of the PVA capping agent. While such analysis may indicate that the relatively limited activity of the dried-only sample towards cyclohexanone ammoximation can be

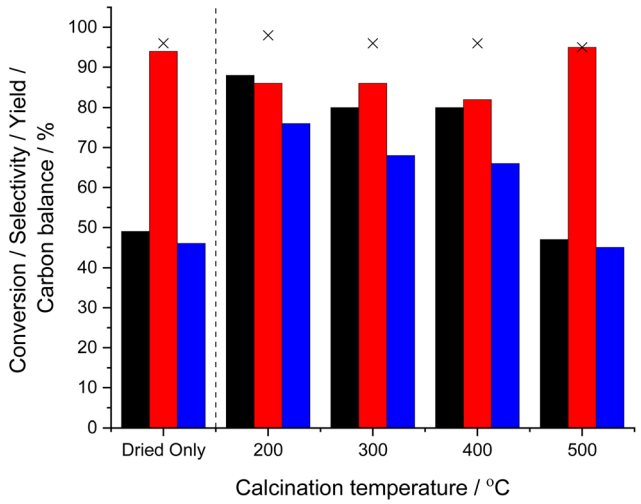

Fig. 4 Effect of calcination temperature on catalytic activity of the 0.33%Au–0.33%Pd/TS-1 catalyst activity towards the ammoximation of cyclohexanone oxime *via in situ* H_2O_2 synthesis. Ammoximation reaction conditions: cyclohexanone (2 mmol), NH_4HCO_3 (4 mmol), $5\%H_2/N_2$ (420 psi), $25\%O_2/N_2$ (160 psi), catalyst (0.075 g), *t*-BuOH (5.9 g), H_2O (7.5 g), 3 h, 80 °C 800 rpm. Key: cyclohexanone conversion (black bar), selectivity towards oxime (red bar), cyclohexanone oxime yield (blue bar), carbon balance (crosses). Note: the dried-only material was exposed to low-temperature oxidative heat treatment (110 °C, 16 h, static air) prior to use.

associated with the presence of the organic overlayer, possibly limiting reagent availability at metal active sites, it is important to note the high activity of the catalyst towards H_2O_2 production. As such it is considered that the presence of the ligand is not the underlying cause for the limited activity of the dried-only material.

We have recently reported that the formation of AuPd alloys is crucial in achieving both high catalytic performance and improved stability during application in the *in situ* ammoximation of cyclohexanone.[18] Notably, in this previous study the AuPd/TS-1 catalyst, which was synthesised *via* a wet impregnation process, displayed a degree of nanoparticle inhomogeneity, typical of the route to catalyst preparation.[10] These concerns around poor control of nanoparticle composition can be largely avoided through colloidal approaches to catalyst synthesis and it can be considered that AuPd alloys are the predominant species present within the 0.33%Au–0.33%Pd/TS-1 (PVA : metal = 1.2) catalyst, regardless of calcination temperature. However, one could also expect the presence of a minority of elementally segregated Au- and Pd-only species, although to a far lesser extent than that observed in the impregnation prepared analogue. As such, and informed by the observation of metal leaching during the H_2O_2 direct synthesis reaction (Table S.6†), we consider that it is possible to attribute the limited ammoximation activity of the dried-only catalyst to a combination of metal leaching and incomplete alloy formation. However, further study is still required to determine the extent to which each factor is responsible for the observed reactivity.

Table 3 Effect of calcination temperature on the mean particle size of the 0.33%Au–0.33%Pd/TS-1 catalyst, prepared *via* sol-immobilisation (PVA : metal = 1.2)

Calcination temperature/°C	Mean particle size/nm (S.D)	Productivity[a]/ $mol_{H2O2}\ kg_{cat}^{-1}\ h^{-1}$	Oxime yield[b]/%
Dried only[c]	2.5 (0.84)	212	46
200	3.4 (1.09)	176	76
300	3.5 (1.02)	138	68
400	3.4 (1.10)	104	66
500	3.5 (0.98)	98	54

[a] H_2O_2 direct synthesis reaction conditions: catalyst (0.01 g), H_2O (2.9 g), MeOH (5.6 g), $5\%H_2/CO_2$ (420 psi), $25\%O_2/CO_2$ (160 psi), 0.5 h, 2 °C, 1200 rpm. [b] Ammoximation reaction conditions: cyclohexanone (2 mmol), NH_4HCO_3 (4 mmol), $5\%H_2/N_2$ (420 psi), $25\%O_2/N_2$ (160 psi), catalyst (0.075 g), *t*-BuOH (5.9 g), H_2O (7.5 g), 3 h, 80 °C, 800 rpm. [c] Dried only sample exposed to 110 °C, 16 h, static air.

Evaluation of the catalytic series by TEM (Table 3, with corresponding micrographs reported in Fig. S.8†), revealed a relatively minor increase in mean particle size upon exposure to high-temperature calcination, which is indicative of the strong interaction between the nanoalloys and catalyst support, under non-reaction conditions, and is in keeping with our evaluation of $AuPd/TiO_2$ catalysts, prepared by a similar synthesis route.[59] However, it is important to note that due to limits of detection it was not possible to rule out the presence of atomic species or metal clusters and indeed the presence of such species may be expected given the high rates of H_2O_2 degradation observed, particularly over the dried material. Perhaps as expected given the oxidative heat treat-

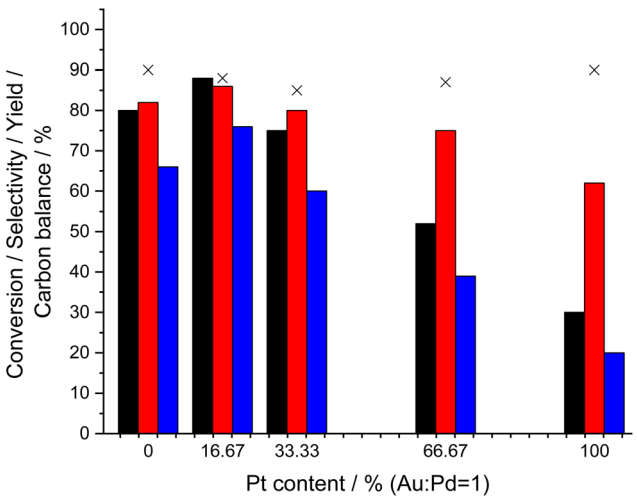

Fig. 5 Effect of Pt incorporation on the catalytic activity of 0.66%AuPd/TS-1 catalysts towards the ammoximation of cyclohexanone oxime *via in situ* H_2O_2 synthesis. Ammoximation reaction conditions: cyclohexanone (2 mmol), NH_4HCO_3 (4 mmol), $5\%H_2/N_2$ (420 psi), $25\%O_2/N_2$ (160 psi), catalyst (0.075 g), *t*-BuOH (5.9 g), H_2O (7.5 g), 3 h, 80 °C 800 rpm. Key: cyclohexanone conversion (black bar), selectivity towards oxime (red bar), cyclohexanone oxime yield (blue bar), carbon balance (crosses). Note: all catalysts were exposed to oxidative heat treatment prior to use (static air, 400 °C, 3 h).

ment utilised, XPS analysis demonstrates a shift in Pd speciation from Pd^0 in the as-prepared, dried catalyst towards a mixed Pd^0–Pd^{2+} state in those materials exposed to calcination (Table S.7†). This coincides with a significant decrease in catalytic activity towards H_2O_2 degradation (Table S.5†), notably the H_2O_2 degradation rate of the dried only catalyst is exceptionally high under conditions optimised for H_2O_2 selectivity (637 mol_{H2O2} kg_{cat}^{-1} h^{-1}), with this metric decreasing substantially upon calcination. As such it is possible to consider that while catalytic activity towards H_2O_2 production is a key metric in oxime production there is also a need to minimise competitive H_2O_2 degradation pathways which involve precious metal nanoalloys. This is likely to be particularly pertinent if the ability of the TS-1 component to utilise H_2O_2 in the formation of hydroxylamine limits overall process efficiency.

The inclusion of dopant concentrations of transition metals, in particular Pt, into supported Pd and AuPd catalysts has been reported to greatly enhance catalytic performance towards a range of chemical transformations,[62,63] including the direct synthesis of H_2O_2.[22,64–67] With these earlier works in mind, we subsequently investigated the effect of Pt incorporation on catalytic performance. A considerable increase in H_2O_2 synthesis rate was observed upon the inclusion of relatively low concentrations of Pt (0.11 wt%) into the 0.66%AuPd/

Table 4 Effect of Pt incorporation on the mean particle size of the 0.66%AuPd/TS-1 catalyst, prepared *via* sol-immobilisation (PVA : metal = 1.2)

Catalyst	Mean particle size/nm (S.D)	Productivity[a]/mol_{H2O2} kg_{cat}^{-1} h^{-1}	Oxime yield[b]/%
0.33%Au–0.33%Pd/TS-1	3.4 (1.10)	104	66
0.275%Au–0.275%Pd–0.11%Pt/TS-1	2.7 (0.66)	135	76
0.22%Au–0.22%Pd–0.22%Pt/TS-1	3.0 (0.98)	106	60
0.11%Au–0.11%Pd–0.44%Pt/TS-1	3.1 (0.75)	72	39
0.66%Pt/TS-1	3.1 (1.25)	58	20

[a] H_2O_2 direct synthesis reaction conditions: catalyst (0.01 g), H_2O (2.9 g), MeOH (5.6 g), 5%H_2/CO_2 (420 psi), 25%O_2/CO_2 (160 psi), 0.5 h, 2 °C, 1200 rpm. [b] Ammoximation reaction conditions: cyclohexanone (2 mmol), NH_4HCO_3 (4 mmol), 5%H_2/N_2 (420 psi), 25%O_2/N_2 (160 psi), catalyst (0.075 g), *t*-BuOH (5.9 g), H_2O (7.5 g), 3 h, 80 °C, 800 rpm. Note: all catalysts were exposed to an oxidative heat treatment prior to use (static air, 400 °C, 3 h).

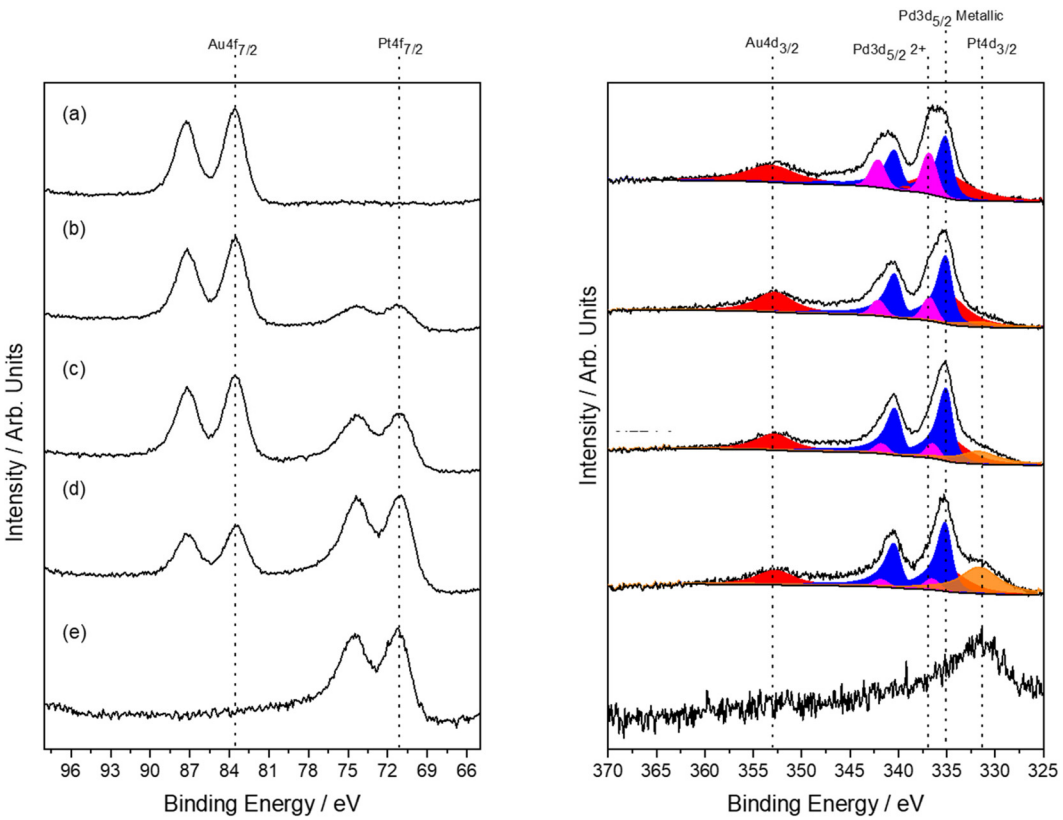

Fig. 6 XPS Au(4f)/Pt(4f) and Pd(3d)/Au(4d) spectra for as-prepared 0.66%AuPdPt/TS-1 catalysts, prepared by sol-immobilisation (PVA : metal = 1.2). (a) 0.33%Au–0.33%Pd/TS-1, (b) 0.275%Au–0.275%Pd–0.11%Pt/TS-1, (c) 0.22%Au–0.22%Pd–0.22%Pt/TS-1 (d) 0.11%Au–0.11%Pd–0.44%Pt/TS-1 and (e) 0.66%Pt/TS-1. Note: all catalysts were exposed to an oxidative heat treatment prior to use (static air, 400 °C, 3 h).

TS-1 catalyst (135 mol_{H2O2} kg_{cat}^{-1} h^{-1}), coinciding with a decrease in H_2O_2 degradation rate (172 mol_{H2O2} kg_{cat}^{-1} h^{-1}) (Table S.8†). Correlating well with catalytic trends observed for H_2O_2 direct synthesis, the 0.275%Au–0.275%Pd–0.11%Pt/TS-1 catalyst was found to offer improved yields of cyclohexanone oxime (76%), with this metric decreasing substantially with further Pt incorporation (Fig. 5). Again, this highlights the close relationship between catalyst activity towards H_2O_2 production and the ammoximation of cyclohexanone. The enhanced activity of the optimal AuPdPt/TS-1 catalyst is further highlighted through comparison of apparent reaction rates (Table S.9†).

Earlier works investigating the promotive effects of Pt incorporation into AuPd nanoalloys have typically focussed on a wet co-impregnation route to catalyst synthesis[60] and as such it has been difficult to determine the key parameters responsible for the enhancement in activity upon the introduction of the dopant, with the modification of Pd oxidation states and changes in nanoparticle size proposed as possible causes for the observed improvement in catalytic performance. However, owing to the increased control offered by the sol-immobilisation route to catalyst synthesis, it is possible to rule out the latter as the cause for the observed catalytic trends, with negligible changes in mean particle size observed across the catalytic series (Table 4, with corresponding micrographs reported in Fig. S.9†).

Analysis of the as-prepared, 0.66%AuPdPt/TS-1 catalysts by XPS is reported in Fig. 6. Upon the introduction of Pt the surface Pd: Au ratio was found to remain largely unchanged, however, perhaps more interestingly a considerable increase in Pd^0 content was observed with the introduction of low concentrations of the dopant, which coincides with an enhancement in catalytic activity towards H_2O_2 (Table S.8†) and production of cyclohexanone oxime (Fig. 5), with Pd^0 content continuing to increase upon further Pt incorporation. Again, in keeping with our earlier studies within this work, these observations clearly highlight the inherent relationship between H_2O_2 production and cyclohexanone ammoximation.

While the catalysts developed within this study have been demonstrated to offer high yields of cyclohexanone oxime, the need to improve catalytic performance, in particular selectivity towards the desired product is clear. With the comparatively high H_2O_2 degradation rates observed over the precious metal-loaded catalysts identified, under conditions considered optimal for H_2O_2 stability, the unselective catalytic formation of H_2O from H_2O_2 *via* hydrogenation and decomposition pathways must also be considered a key factor in overall ammoximation process efficiency. Indeed, in order to rival the current route to cyclohexanone oxime production the selective utilisation of H_2 is a key parameter to consider and may be achieved through better balancing rates of H_2O_2 synthesis, over the active metal surfaces, and the subsequent utilisation of the synthesised H_2O_2 in the formation of the hydroxylamine intermediate. Returning to the 0.33%Au–0.33%Pd/TS-1 (PVA : metal = 1.2) catalyst, additional bare TS-1 (0.075 g) was used in conjunction with the metal-loaded catalyst, with a resulting

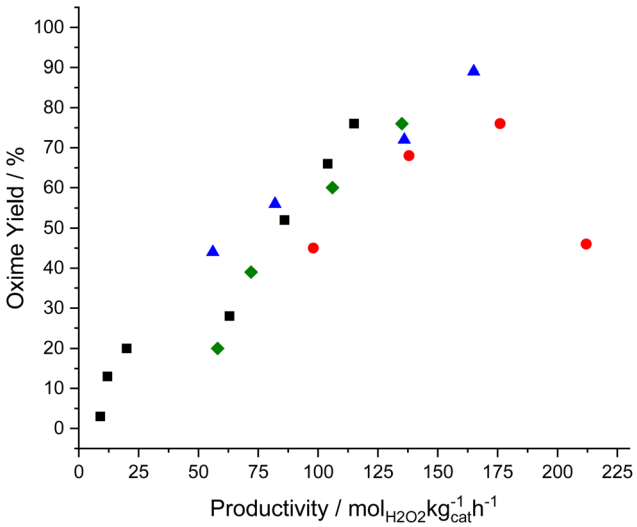

Fig. 7 The relationship between catalytic activity towards the direct synthesis of H_2O_2 and the *in situ* ammoximation of cyclohexanone. H_2O_2 direct synthesis reaction conditions: catalyst (0.01 g), H_2O (2.9 g), MeOH (5.6 g), 5%H_2/CO_2 (420 psi), 25%O_2/CO_2 (160 psi), 0.5 h, 2 °C, 1200 rpm. Ammoximation reaction conditions: cyclohexanone (2 mmol), NH_4HCO_3 (4 mmol), 5%H_2/N_2 (420 psi), 25%O_2/N_2 (160 psi), catalyst (0.075 g), *t*-BuOH (5.9 g), H_2O (7.5 g), 3 h, 80 °C, 800 rpm. Key: 0.66%AuPd/TS-1 catalysts with varying Au : Pd ratio (black squares), varying the calcination temperature of the 0.33%Au–0.33%Pd/TS-1 (PVA : metal = 1.2) catalyst (red circles), varying the PVA : metal ratio of the 0.33%Au–0.33%Pd/TS-1 catalysts (blue triangles), varying Pt content in 0.66%AuPdPt/TS-1 catalysts (green diamonds).

improvement in overall efficacy (oxime yield = 93%) compared to that observed when using AuPd/TS-1 alone (oxime yield = 66%) (Fig. S.10†). We consider that this highlights the need for the iterative development of both catalytically active centres (*i.e.*, the metal nanoparticles and Ti^{IV} within the TS-1 framework), and may direct attention towards the utilisation and development of titanosilicates with more readily accessible Ti^{IV} centres than those within TS-1.[68–71]

Finally, the relationship between catalytic performance towards the direct synthesis of H_2O_2 and *in situ* cyclohexanone ammoximation was compared, with a strong correlation between the two distinct reaction pathways observed (Fig. 7). Such observations may direct future attention towards the improvement of catalyst activity towards H_2O_2, potentially at the cost of selectivity. However, our studies have also revealed the need to minimise competitive H_2O_2 degradation pathways while also ensuring the efficacy of the overall ammoximation process does not become limited by the ability of the TS-1 component to synthesise hydroxylamine.

Conclusion

The *in situ* synthesis of H_2O_2 from molecular H_2 and O_2 is demonstrated to offer an efficient route to the formation of cyclohexanone oxime, a major precursor to Nylon-6. With a focus on a composite TS-1 based catalyst, prepared *via* a sol-

immobilisation protocol the need to improve both H_2O_2 synthesis rates through control of the precious metal component, in addition to the ability of the titanosilicate to readily utilise the synthesised H_2O_2 is identified. In particular, the role of alloying Pd with Au and the introduction of relatively small concentrations of Pt into AuPd nanoparticles are both revealed as measures which promote the synthesis of H_2O_2 and *in situ* production of the oxime.

Author contributions

R.J.L, K.U and C.B.P conducted catalyst synthesis, testing, and data analysis. R.J.L, T.E.D, D.J.M and C.B.P conducted catalyst characterisation and corresponding data processing. R.J.L, K. U, Y.F, J.S, J.K.E, S.J.F, Y.Y, and G.J.H contributed to the design of the study and provided technical advice and result interpretation. R.J.L wrote the manuscript and supporting information, with all authors commenting on and amending both documents. All authors discussed and contributed to this work.

Conflicts of interest

The authors declare no conflict of interest.

Acknowledgements

The authors wish to thank UBE Corporation for financial support. R. J. L and G. J. H acknowledge the Max Planck Centre for Fundamental Heterogeneous Catalysis (FUNCAT) for financial support. In addition, S. J. F acknowledges the award of a Prize Research Fellowship from the University of Bath. XPS data collection was performed at the EPSRC National Facility for XPS ('Harwell XPS'). Operated by Cardiff University and UCL, under contract no. PR16195. The authors would like to thank the CCI-Electron Microscopy Facility which has been part-funded by the European Regional Development Fund through the Welsh Government and The Wolfson Foundation.

References

1 HDIN Research, Global Nylon 6 production capacity to reach 8.86 million tons in 2024 (2022) **https://www.hdinresearch.com/news/56**.
2 P. Roffia, G. Leofanti, A. Cesana, M. Mantegazza, M. Padovan, G. Petrini, S. Tonti and P. Gervasutti, *Stud. Surf. Sci. Catal.*, 1990, **55**, 43–52.
3 A. Zecchina, S. Bordiga, C. Lamberti, G. Ricchiardi, C. Lamberti, G. Ricchiardi, D. Scarano, G. Petrini, G. Leofanti and M. Mantegazza, *Catal. Today*, 1996, **32**, 97–106.
4 R. J. Lewis and G. J. Hutchings, *ChemCatChem*, 2019, **11**, 298–308.
5 J. R. Scoville and I. A. Novicova (Cottrell Ltd.), US 5900256, 1996.
6 G. Gao, Y. Tian, X. Gong, Z. Pan, K. Yong and B. Zong, *Chin. J. Catal.*, 2020, **41**, 1039–1047.
7 J. K. Edwards, B. Solsona, E. N. Ntainjua, A. F. Carley, A. A. Herzing, C. J. Kiely and G. J. Hutchings, *Science*, 2009, **323**, 1037–1041.
8 N. M. Wilson, P. Priyadarshini, S. Kunz and D. W. Flaherty, *J. Catal.*, 2018, **357**, 163–175.
9 J. Brehm, R. J. Lewis, D. J. Morgan, T. E. Davies and G. J. Hutchings, *Catal. Lett.*, 2021, **152**, 254–262.
10 C. M. Crombie, R. J. Lewis, D. Kovačič, D. J. Morgan, T. E. Davies, J. K. Edwards, M. S. Skjøth-Rasmussen and G. J. Hutchings, *Catal. Lett.*, 2020, **151**, 164–171.
11 C. M. Crombie, R. J. Lewis, R. L. Taylor, D. J. Morgan, T. E. Davies, A. Folli, D. M. Murphy, J. K. Edwards, J. Qi, H. Jiang, C. J. Kiely, X. Liu, M. S. Skjøth-Rasmussen and G. J. Hutchings, *ACS Catal.*, 2021, **11**, 2701–2714.
12 Z. Jin, L. Wang, E. Zuidema, K. Mondal, M. Zhang, J. Zhang, C. Wang, X. Meng, H. Yang, C. Mesters and F. Xiao, *Science*, 2020, **367**, 193–197.
13 R. J. Lewis, A. Bara-Estaun, N. Agarwal, S. J. Freakley, D. J. Morgan and G. J. Hutchings, *Catal. Lett.*, 2019, **149**, 3066–3075.
14 L. Torrente-Murciano, T. Villager and D. Chadwick, *ChemCatChem*, 2015, **7**, 925–927.
15 Q. Chen and E. J. Beckman, *Green Chem.*, 2008, **10**, 934–938.
16 G. Dodekatos, L. Abis, S. J. Freakley, H. Tüysüz and G. J. Hutchings, *ChemCatChem*, 2018, **10**, 1351–1359.
17 G. Wang, W. Du, X. Duan, Y. Cao, Z. Zhang, J. Xu, W. Chen, G. Qian, W. Yuan, X. Zhou and D. Chen, *Chem. Catal.*, 2021, **1**, 885–895.
18 R. J. Lewis, K. Ueura, X. Liu, Y. Fukuta, T. E. Davies, D. J. Morgan, L. Chen, J. Qi, J. Singleton, J. K. Edwards, S. J. Freakley, C. J. Kiely, Y. Yamamoto and G. J. Hutchings, *Science*, 2022, **376**, 615–620.
19 T. Richards, R. J. Lewis, D. J. Morgan and G. J. Hutchings, *Catal. Lett.*, 2022, DOI: **10.1007/s10562-022-03967-8**.
20 J. K. Edwards, A. F. Carley, A. A. Herzing, C. J. Kiely and G. J. Hutchings, *Faraday Discuss.*, 2008, **138**, 225–239.
21 L. M. Rossi, J. L. Fiorio, M. A. S. Garcia and C. P. Ferraz, *Dalton Trans.*, 2018, **47**, 5889–5915.
22 X. Gong, R. J. Lewis, S. Zhou, D. J. Morgan, T. E. Davies, X. Liu, C. J. Kiely, B. Zong and G. J. Hutchings, *Catal. Sci. Technol.*, 2020, **10**, 4635–4644.
23 A. Villa, D. Wang, G. M. Veith, F. Vindigni and L. Prati, *Catal. Sci. Technol.*, 2013, **3**, 3036–3041.
24 G. M. Lari, B. Puértolas, M. Shahrokhi, N. López and J. Pérez-Ramírez, *Angew. Chem., Int. Ed.*, 2017, **56**, 1775–1779.
25 R. J. Lewis, M. Koy, M. Macino, M. Das, J. H. Carter, D. J. Morgan, T. E. Davies, J. B. Ernst, S. J. Freakley, F. Glorius and G. J. Hutchings, *J. Am. Chem. Soc.*, 2022, **144**(34), 15431–15436.

26 C. B. Paris, A. G. Howe, R. J. Lewis, D. Hewes, D. J. Morgan, Q. He and J. K. Edwards, *ACS Catal.*, 2022, **12**, 4440–4454.
27 A. Santos, R. J. Lewis, G. Malta, A. G. R. Howe, D. J. Morgan, E. Hampton, P. Gaskin and G. J. Hutchings, *Ind. Eng. Chem. Res.*, 2019, **58**, 12623–12631.
28 S. J. Freakley, R. J. Lewis, D. J. Morgan, J. K. Edwards and G. J. Hutchings, *Catal. Today*, 2015, **248**, 10–17.
29 M. Chen, D. Kumar, C.-W. Yi and D. W. Goodman, *Science*, 2005, **310**, 291–293.
30 J. K. Edwards, J. Pritchard, L. Lu, M. Piccinini, G. Shaw, A. F. Carley, D. J. Morgan, C. J. Kiely and G. J. Hutchings, *Angew. Chem., Int. Ed.*, 2014, **53**, 2381–2384.
31 N. M. Wilson, P. Priyadarshini, S. Kunz and D. W. Flaherty, *J. Catal.*, 2018, **357**, 163–175.
32 T. Ricciardulli, S. Gorthy, J. S. Adams, C. Thompson, A. M. Karim, M. Neurock and D. W. Flaherty, *J. Am. Chem. Soc.*, 2021, **143**, 5445–5464.
33 J. Li, T. Ishihara and K. Yoshizawa, *J. Phys. Chem. C*, 2011, **115**, 25359–25367.
34 T. Richards, J. H. Harrhy, R. J. Lewis, A. G. R. Howe, G. M. Suldecki, A. Folli, D. J. Morgan, T. E. Davies, E. J. Loveridge, D. A. Crole, J. K. Edwards, P. Gaskin, C. J. Kiely, Q. He, D. M. Murphy, J. Maillard, S. J. Freakley and G. J. Hutchings, *Nat. Catal.*, 2021, **4**, 575–585.
35 J. M. Campos-Martin, G. Blanco-Brieva and J. L. Fierro, *Angew. Chem., Int. Ed.*, 2006, **45**, 6962–6984.
36 C. J. Wrasman, A. Boubnov, A. R. Riscoe, A. S. Hoffman, S. R. Bare and M. Cargnello, *J. Am. Chem. Soc.*, 2018, **140**, 12930–12939.
37 S. Han and C. B. Mullins, *ACS Catal.*, 2018, **8**, 3641–3649.
38 S. Han and C. B. Mullins, *Acc. Chem. Res.*, 2021, **54**, 379–387.
39 Y. Han, Z. Zhong, K. Ramesh, F. Chen, L. Chen, T. White, Q. Tay, S. N. Yaakub and Z. Wang, *J. Phys. Chem. C*, 2007, **111**, 8410–8413.
40 F. Gao, Y. Wang and D. W. Goodman, *J. Am. Chem. Soc.*, 2009, **131**, 5734–5735.
41 F. Gao and D. W. Goodman, *Chem. Soc. Rev.*, 2012, **41**, 8009–8020.
42 J. Li, T. Ishihara and K. Yoshizawa, *J. Phys. Chem. C*, 2011, **115**, 7392–7398.
43 P. Tian, D. Ding, Y. Sun, F. Xuan, X. Xu, J. Xu and Y. Han, *J. Catal.*, 2019, **369**, 95–104.
44 P. Tian, L. Ouyang, X. Xu, C. Ao, X. Xu, R. Si, X. Shen, M. Lin, J. Xu and Y. Han, *J. Catal.*, 2017, **349**, 30–40.
45 C. Williams, J. H. Carter, N. F. Dummer, Y. K. Chow, D. J. Morgan, S. Yacob, P. Serna, D. J. Willock, R. J. Meyer, S. H. Taylor and G. J. Hutchings, *ACS Catal.*, 2018, **8**, 2567–2576.
46 L. F. de L. e Freitas, B. Puértolas, J. Zhang, B. Wang, A. S. Hoffman, S. R. Bare, J. Pérez-Ramírez, J. W. Medlin and E. Nikolla, *ACS Catal.*, 2020, **10**, 5202–5207.
47 S. J. Freakley, N. Agarwal, R. U. McVicker, S. Althahban, R. J. Lewis, D. J. Morgan, N. Dimitratos, C. J. Kiely and G. J. Hutchings, *Catal. Sci. Technol.*, 2020, **10**, 5935–5944.
48 S. Abate, K. Barbera, G. Centi, G. Giorgianni and S. Perathoner, *J. Energy Chem.*, 2016, **25**, 297–305.
49 R. J. Lewis, E. N. Ntainjua, D. J. Morgan, T. E. Davies, A. F. Carley, S. J. Freakley and G. J. Hutchings, *Catal. Commun.*, 2021, **161**, 106358.
50 G. K. Wertheim, S. B. DiCenzo and D. N. E. Buchanan, *Phys. Rev. B: Condens. Matter Mater. Phys.*, 1986, **33**, 5384–5390.
51 D. R. Jones, S. Iqbal, P. J. Miedziak, D. J. Morgan, J. K. Edwards, Q. He and G. J. Hutchings, *Top. Catal.*, 2018, **61**, 833–843.
52 J. A. Lopez-Sanchez, N. Dimitratos, C. Hammond, G. L. Brett, L. Kesavan, S. White, P. Miedziak, R. Tiruvalam, R. L. Jenkins, A. F. Carley, D. Knight, C. J. Kiely and G. J. Hutchings, *Nat. Chem.*, 2011, **3**, 551–556.
53 Y. Borodko, H. S. Lee, S. H. Joo, Y. Zhang and G. Somorjai, *J. Phys. Chem. C*, 2010, **114**, 1117–1126.
54 L. R. Baker, G. Kennedy, J. M. Krier, M. Van Spronsen, R. M. Onorato and G. A. Somorjai, *Catal. Lett.*, 2012, **142**, 1286–1294.
55 Y. Zhao, L. Jia, J. A. Medrano, J. R. H. Ross and L. Lefferts, *ACS Catal.*, 2013, **3**, 2341–2352.
56 S. Cattaneo, S. J. Freakley, D. J. Morgan, M. Sankar, N. Dimitratos and G. J. Hutchings, *Catal. Sci. Technol.*, 2018, **8**, 1677–1685.
57 J. C. Matsubu, S. Zhang, L. DeRita, N. S. Marinkovic, J. G. Chen, G. W. Graham, X. Pan and P. Christopher, *Nat. Chem.*, 2017, **9**, 120–127.
58 J. K. Edwards, J. Pritchard, M. Piccinini, G. Shaw, Q. He, A. F. Carley, C. J. Kiely and G. J. Hutchings, *J. Catal.*, 2012, **292**, 227–238.
59 J. Pritchard, M. Piccinini, R. Tiruvalam, Q. He, N. Dimitratos, J. A. Lopez-Sanchez, D. J. Morgan, A. F. Carley, J. K. Edwards, C. J. Kiely and G. J. Hutchings, *Catal. Sci. Technol.*, 2013, **3**, 308–317.
60 R. J. Lewis, K. Ueura, Y. Fukuta, S. J. Freakley, L. Kang, R. Wang, Q. He, J. K. Edwards, D. J. Morgan, Y. Yamamoto and G. J. Hutchings, *ChemCatChem*, 2019, **11**, 1673–1680.
61 Y. K. Chow, N. F. Dummer, J. H. Carter, R. J. Meyer, R. D. Armstrong, C. Williams, G. Shaw, S. Yacob, M. M. Bhasin, D. J. Willock, S. H. Taylor and G. J. Hutchings, *ChemPhysChem*, 2018, **19**, 402–411.
62 S. A. Kondrat, P. J. Miedziak, M. Douthwaite, G. L. Brett, T. E. Davies, D. J. Morgan, J. K. Edwards, D. W. Knight, C. J. Kiely, S. H. Taylor and G. J. Hutchings, *ChemSusChem*, 2014, **7**, 1326–1334.
63 J. W. M. Crawley, I. E. Gow, N. Lawes, I. Kowalec, L. Kabalan, C. R. A. Catlow, A. J. Logsdail, S. H. Taylor, N. F. Dummer and G. J. Hutchings, *Chem. Rev.*, 2022, **122**, 6795–6849.
64 G. Bernardotto, F. Menegazzo, F. Pinna, M. Signoretto, G. Cruciani and G. Strukul, *Appl. Catal., A*, 2009, **358**, 129–135.
65 S. Quon, D. Y. Jo, G.-H. Han, S. S. Han, M. Seo and K. Lee, *J. Catal.*, 2018, **368**, 237–247.

66 T. Deguchi, H. Yamano, S. Takenouchi and M. Iwamoto, *Catal. Sci. Technol.*, 2018, **8**, 1002–1015.
67 H. V. Nguyen, K. Y. Kim, H. Nam, S. Y. Lee, T. Yu and T. S. Seo, *Lab Chip*, 2020, **20**, 3293–3301.
68 J. Ding and P. Wu, *Appl. Catal., A*, 2014, **488**, 86–95.
69 F. Song, Y. Liu, L. Wang, H. Zhang, M. He and P. Wu, *Appl. Catal., A*, 2007, **327**, 22–31.
70 S. Zhao, W. Xie, J. Yang, Y. Liu, Y. Zhang, B. Xu, J. Jiang, M. He and P. Wu, *Appl. Catal., A*, 2011, **394**, 1–8.
71 J. S. Reddy, S. Sivasanker and P. Ratnasamy, *J. Mol. Catal.*, 1991, **69**, 383–392.